applied optics

Dielectric microsphere sizing using fluorescence microscopy of whispering gallery mode resonances from adsorbed dyes

Azizeh Alidoust Ghatar, Nitay Ben-Shachar, and Eric C. Le Ru*

The MacDiarmid Institute for Advanced Materials and Nanotechnology, School of Chemical and Physical Sciences, Victoria University of Wellington, P.O. Box 600, Wellington 6140, New Zealand
**eric.leru@vuw.ac.nz*

Received 12 September 2024; revised 19 October 2024; accepted 27 October 2024; posted 28 October 2024; published 12 November 2024

Whispering gallery mode (WGM) resonances in dielectric microspheres are very sensitive to their size and environment, which can be used for sensing but also as an indirect proxy to determine their size. By coating them with suitable fluorescent dyes and using fluorescence microscopy, we show that the WGM resonances of individual microspheres in solution can be easily studied with a high throughput. Brownian motion ensures that a representative sample is probed over time in the scattering volume. To analyze these WGM-imprinted fluorescent spectra, we propose a simple algorithm based on monitoring the spacing between resonances and comparing it to Mie theory predictions to infer their size. This allows us to measure the size distribution of typical polystyrene microsphere solutions. We also discuss the potential effects of dye concentration and choice of particle refractive index on the analysis. This method can be used, for example, for quality-testing microsphere solutions. © 2024 Optica Publishing Group. All rights, including for text and data mining (TDM), Artificial Intelligence (AI) training, and similar technologies, are reserved.

https://doi.org/10.1364/AO.541870

1. INTRODUCTION

Dielectric microspheres (MSs) are used in diverse applications, including for drug release [1], as models for the optical properties of biological tissues [2] or climate-related aerosols [3], as biosensors [4–7], as fluorescent tags in biological studies [8], as microcavity resonators [9], or as lasers [7,10–12]. In many of these studies the particle size and size distribution are crucial parameters. These can be conveniently monitored using dynamic light scattering (DLS), but the accuracy of this technique remains limited [13,14]. For fundamental studies, it is also sometimes necessary to measure the size of an individual microsphere. For this, a more advanced approach is via the measurement of the optical resonance structure of the MSs. MSs can indeed exhibit under the right conditions very sharp resonance peaks in their optical properties. These are generally called whispering gallery modes (WGMs) in reference to the analogous sound resonances in circular buildings [15], but are sometimes also referred to as Mie resonances and morphology-dependent resonances. These modes, which can be observed in various materials such as polystyrene [3,12], silicon [16,17], or titanium dioxide [18], have been studied in detail: theoretically in the framework of Mie theory [19–21], and experimentally in various contexts, notably as high-Q cavities. Some of these works have focused specifically on understanding how these modes can be used to infer the size of the MSs. The majority of these experiments have used MSs suspended in air [20,22–26] and measured their scattering or extinction spectra to probe the WGM resonances of a single particle. Various approaches have been used to infer the size, most by correlating the measured peak positions to predictions, either analytical approximations or full Mie theory calculations [25,27–29]. All these studies have focused on one or two particles only.

In this work, we aim to perform such analysis on a large number of polystyrene (PS) MSs in solution in order to accurately extract their size distribution. To achieve this, we use fluorescence microscopy and the concept of an active WGM resonator [7] instead of standard scattering experiments. This approach has only been used sporadically before. Some groups have used MSs with dyes embedded inside them [30,31], but this only applies to particles manufactured for that purpose; it cannot be done easily on existing MSs [32]. Here we instead coat the MSs with a suitable fluorophore, whose fluorescence spectrum is then modified by the presence of the WGMs and clearly reveals their structure [33,34]. This approach enables us to probe a large number of MSs, with sampling facilitated by Brownian motion of the MSs in and out of the field of view of the microscope. We also develop a simple automated analysis of the spectra based on monitoring the WGM spacings, instead of their positions. These steps allow us to measure the size distribution of 10 and 15 μm PS MSs to a high accuracy. We also discuss the potential effects of dye concentration on our results and the choice of PS refractive index, which is needed for the Mie theory calculations.

2. METHODS

Dye-coated microsphere solutions. Polystyrene microspheres were obtained from Duke Scientific with nominal radii of 10 ± 0.9 μm and 14.6 ± 0.5 μm and stock concentration of 1% (w/w). These were diluted in ultrapure water 100 times for 10 μm MS and 25 times for 14.6 μm MS. Rhodamine 6G (R6G) powder (Sigma) was diluted in ultrapure water to a 10 μM stock solution. Then 10 μL of this R6G solution was added to 990 μL of the diluted PS solution to give a final R6G concentration of 100 nM. Similar dye-coated solutions were also prepared from a 12 μM Nile Blue (A) solution (with 120 nM final concentration). These positively charged dyes are expected to adsorb on the PS MS via electrostatic interaction.

Fluorescence measurements. Fluorescence spectra were measured in solution using a ×20 water immersion objective for excitation and collection (in backscattering). We used a Labram HR800 Raman spectrometer with laser excitation at 514.5 nm or 633.2 nm, nitrogen-cooled CCD-detector, and a 300 l/mm grating, which provided a good compromise between the range of measured wavelengths and the spectral resolution (about $2-3\ \mathrm{cm}^{-1}$ or 0.1 nm). Laser power was 0.04 mW and spectra were acquired continuously with 0.5 s integration time. The area of the beam at focus is estimated to be ~40 $\mu\mathrm{m}^2$ and the height of the scattering volume 200 μm giving an effective scattering volume [35] of 8000 $\mu\mathrm{m}^3$.

Particle concentrations. From these numbers, we estimate the particle concentration in the final solutions to be 1.8×10^8 MSs/L for the 10 μm MSs and 2.3×10^8 MSs/L for 14.6 μm MSs. The average number of MSs in the scattering volume is therefore of the order of 0.0016. Most of the spectra are therefore without MS, but thanks to Brownian motion, we observe occasional events corresponding to one MS crossing the scattering volume. These are clearly identifiable as they are larger than the background fluorescence spectrum from unadsorbed molecules and usually exhibit a clear resonance structure; see Fig. 1. On average, we observe ~10−15 events per 1000 spectra, which is somewhat larger than what these simple estimates would have suggested.

Dye coverage. Given the dye concentration, the maximum coverage for 100% adsorption is of the order of 3×10^8 dye/MS or about $\rho = 1$ dye/nm^2 on the 10 μm MSs coated with 100 nM rhodamine. However, from the observed background fluorescence (Fig. 1), we deduce that the equivalent of 75 nM R6G is not adsorbed on the MS, so the R6G coverage is actually reduced to $\rho \sim 0.25$ dye/nm^2. For the 14.6 μm MS coated with 120 nM Nile Blue, the maximum coverage at 100% adsorption is $\rho = 0.45$ dye/nm^2.

Mie theory calculations. The optical properties of the PS MSs are modeled using Mie theory [36] using the SPlaC codes [37,38]. These include in particular calculations of the surface-averaged local field intensity enhancement factor (LFIEF), which provides a clearer picture of the WGM modes (see below). As the WGM resonances are very sharp, a small spacing of 0.01 nm is used for all spectral calculations. We use literature values for the wavelength dependence of water [39]. For polystyrene, we use the following Cauchy dispersion:

$$n(\lambda) = A + \frac{B}{\lambda^2} + \frac{C}{\lambda^4}, \tag{1}$$

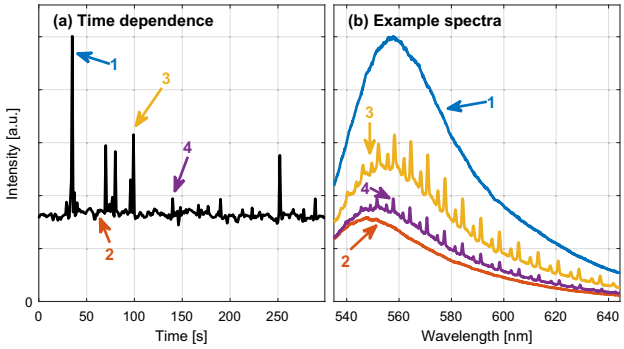

Fig. 1. (a) Integrated intensity of fluorescence as a function of time for R6G-coated 10 μm PS MSs in water. Some individual spectra are identified by a number and shown in (b). Most spectra are similar to spectrum 2 and correspond to the bare fluorescence spectrum of non-adsorbed dyes in the absence of MS. When a MS crosses the scattering volume, a larger fluorescence is observed, most of the time with clear resonances (spectra 3 and 4), but some without are also observed rarely (spectrum 1). The latter may be due to non-spherical particles, abnormally small MS with no WGM resonances in this region, or simply a piece of dust.

with

$$A = 1.56385, \quad B = 0.007855\ \mu\mathrm{m}^2, \quad C = 0.000315\ \mu\mathrm{m}^4.$$

This is the best fit to recent ellipsometric measurements [40], which are also very close to earlier data sets [41,42].

3. RESULTS

A. Inferring Size from Mode Spacing

We start with theoretical predictions from Mie theory to understand the nature of the WGM resonances and how they relate to particle size; see Fig. 2. The far-field optical properties (extinction/scattering spectra) exhibit sharp peaks related to WGM resonances [see Fig. 2(a)], but these are superimposed on broader peaks/oscillations (as usually observed for large dielectric particles), which makes automated analysis more difficult. We therefore instead consider the wavelength-dependent surface-averaged local field intensity enhancement factor, which can be calculated in a similar fashion from Mie coefficients [38]. This factor is central to, for example, surface-enhanced Raman or fluorescence spectroscopy [38] and is more relevant to our experiments. Here, it also provides an easier visualization and automated analysis of the WGM resonances; see Fig. 2(b).

As seen in Figs. 2(a) and 2(b), there are two types of WGMs and the resonances alternate between the two. Within Mie theory, we can show that these correspond to specific multipolar excitations of high multipolar order and the two types relate to the transverse magnetic (TM) or transverse electric (TE) multipoles. Some are identified in Figs. 2(a) and 2(b) for illustration. The linewidth of these peaks is of the order of 0.1 nm, which corresponds to a quality factor of 10^4, which is relatively low compared to other WGM-supporting systems. As evident, the position of these resonances is very sensitive to size, and this has been used previously to infer particle size by matching experimental peak positions to Mie theory predictions [25,27–29].

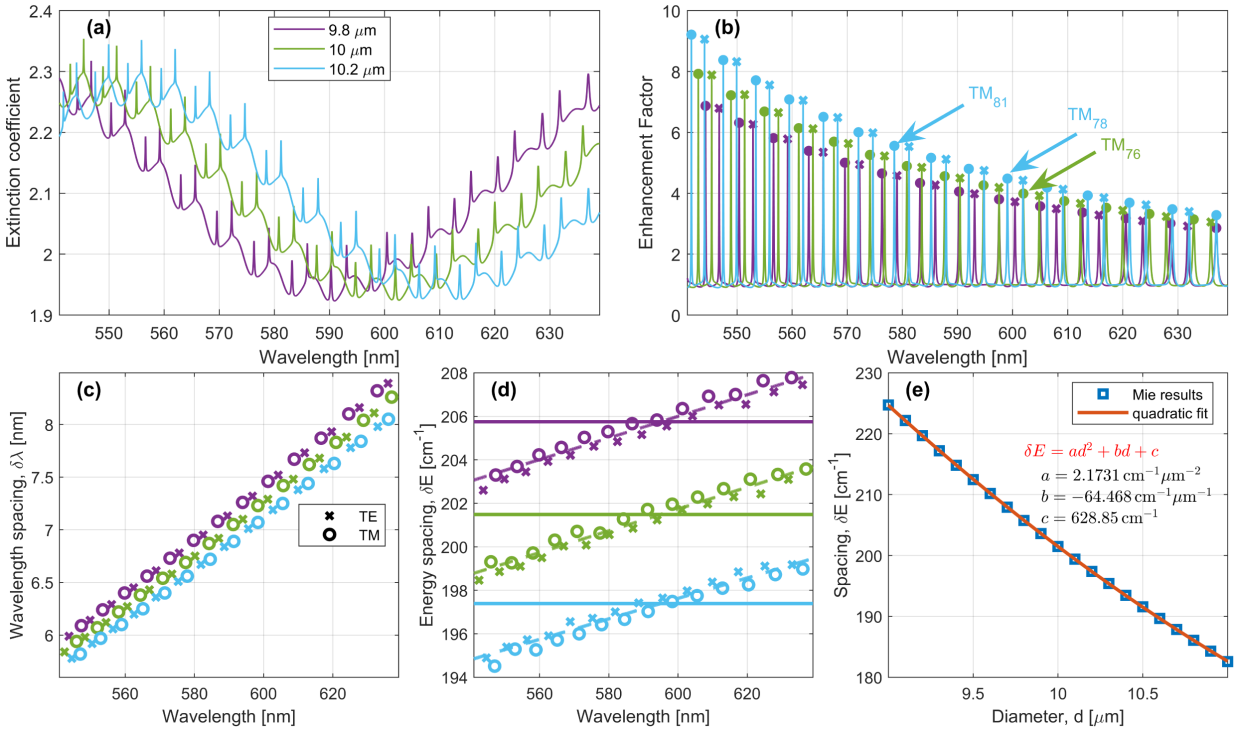

Fig. 2. (a), (b) Calculated extinction spectra (a) and average local field intensity enhancement factor (b) for PS spheres of 9.8, 10, and 10.2 μm diameter in water. The derived locations of the TE (crosses) and TM (circles) resonances are indicated as symbols. (c), (d) Wavelength (c) and energy (d) spacing between consecutive TE or TM resonances as a function of average peak wavelength for each particle. In (d) the energy spacing only increases slightly (dashed line shows linear fit) and the average δE is shown as solid lines. (e) Predicted δE as a function of particle size over the range 9–11 μm and quadratic fit to the data.

This step can be fairly complicated because a small environmental factor can shift the resonance positions and we here propose a simpler approach based on mode spacing (also called free spectral range) instead of peak position.

More specifically, we consider the mode spacing between alternating peaks, in other words between two consecutive TE or TM peaks. As shown in Figs. 2(c) and 2(d), these mode spacings show a well-defined pattern, which is also very sensitive to size. In particular, the mode spacings expressed in energy are almost constant for a given particle; see Fig. 2(d). There is only a small increase with wavelength, which is related to the wavelength dependence of the relative refractive index (without it, one can check that it becomes negligible). These dependencies could also be deduced from analytical expressions for the mode spacing [16,17,20] but we will here keep a fully numerical approach as it will be closer to the analysis we perform on the experimental data.

To correlate energy spacing with size, it is easiest to extract an average spacing. For these 10 μm particles, we have chosen to calculate δE as the average spacing for peaks in the range $550 \le \lambda \le 640$ nm as it matches well our usable experimental data for experiments with R6G excited at 514.5 nm. It should be noted that this average can be written explicitly as

$$\delta E = \frac{1}{N} \sum_{n=1}^{n=N-1} (E_{n+1} - E_n) = \frac{1}{N} [E_N - E_1], \quad \textbf{(2)}$$

where $E_1..E_N$ denote the peak energies in the range of interest. This means that although the individual mode spacing $E_{n+1} - E_n$ may fluctuate because of experimental errors, the uncertainty in δE is only determined by the uncertainty in the position of the first and last peaks in the range and the number of peaks N (of the order of 12–15 here for each of TE/TM). Given our spectral resolution of $\sim 2-3\ \mathrm{cm}^{-1}$, the experimental uncertainty in δE should be of the order $0.2\ \mathrm{cm}^{-1}$ and therefore quite low. An alternative, arguably more robust, way of extracting this average δE is to perform a linear fit of the data over the same range [shown as a dashed line in Fig. 2(d)] and take the value at the mid-point (595 nm in our case). The two approaches give the same δE within $0.2\ \mathrm{cm}^{-1}$ for the theoretical and experimental spectra we have looked at. We have used the second approach (linear fit) in our analysis, but the two approaches appear equivalent in practice. Note that the uncertainty in δE would increase proportionally with the fluorescence spectral resolution, but a much lower resolution could also affect the sharpness of the peaks and therefore the efficiency of the automatic peak-detection algorithm.

The derived average spacings are strongly correlated with particle size. The relationship is close to linear when considering a small range of sizes around 10 μm, but for more precision we approximate it as a quadratic relationship as shown in the example of Fig. 2(e). To determine size, one can then simply measure δE from experiments and deduce the size from it using Fig. 2(e). Given the approximate slope of $-21\ \mathrm{cm}^{-1}/\mu\mathrm{m}$, this amounts to an uncertainty of ~0.01 μm or 0.1% in the size

determination. This method to determine size is summarized in more details in Section S.I. of Supplement 1.

A similar approach can be developed for other particle sizes, as long as clear sharp WGM resonances [as in Fig. 2(b)] can be observed in a wavelength range that can be probed with a fluorescent dye. We here further illustrate this with the case of nominally 14.6 μm PS MSs in water. For these larger particles the WGM resonances around 600 nm show a more complex pattern (with the addition of higher-degree resonances for a given multipolar order). This can be overcome by considering longer wavelengths, in our case the range 670–770 nm. The same analysis can then be carried out as shown in Fig. S1 of Supplement 1.

B. Analysis of a Single Fluorescence Spectrum

We now demonstrate how this size determination method can be applied to fluorescence spectra of dye-coated MSs. Note that the fluorescence method does not rely on resonant excitation of one WGM mode, which could happen if the laser wavelength matches exactly a WGM. Statistically, these would be rare events as both WGM and laser have a narrow linewidth. We therefore believe that the majority of the fluorescence spectra we measure are for non-resonant excitation and the observed variations in fluorescence intensity (see Fig. 1) are related to the position of the MS inside the scattering volume (i.e., centered versus off-centered, at focus versus out-of-focus).

Figure 3 shows example raw fluorescence spectra of two representative R6G-coated MSs of 10 μm diameter. The fluorescence spectrum is stronger than the background fluorescence from unadsorbed R6G molecules, and also appears slightly redshifted. In addition, clear sharp resonances associated with the WGMs are observed. This is analogous to surface-enhanced fluorescence for dyes on metallic nanoparticles, where the fluorescence spectrum is modified and its spectral shape follows the plasmon resonance of the particle [33,43,44]. Here the intrinsic resonances are the WGMs of the sphere, so the resonance structure is reflected in the fluorescence spectral profile. We see two sets of resonances with alternating weaker and stronger resonances. From their spacings, the weaker (stronger) ones can be associated with the TM (TE) modes; this will be discussed elsewhere and is not important to this work. From a closer inspection, we also see that the resonance positions are not the same for the two particles, which is expected because their size is slightly different. Using an automated peak detection algorithm, we can extract peak positions and mode spacings (between consecutive TE and TM peaks), plotted against peak positions in Fig. 3(c). The average mode spacing can be calculated and the particle size deduced as explained in Fig. 2.

A similar analysis can be done for the larger PS spheres (see Fig. S2). Note that the choice of excitation wavelength and wavelength range is important (and size dependent). If peaks from different radial mode orders are present in the region of analysis, this can lead to problems in peak detection and inconsistencies in the measured mode spacing. This would introduce errors when determining the diameter. For 14.6 μm spheres, longer wavelengths are needed to obtain a clean, single-mode-order spectrum, so we use a different fluorescent dye, Nile Blue, excited at 632.8 nm. Otherwise, the analysis and conclusions are very similar.

C. Automatic Extraction of Resonance Positions

In order to analyze more efficiently these spectra, we have developed an algorithm to automatically extract WGM peak positions. We start by normalizing the measured fluorescence spectrum by the background fluorescence of unadsorbed R6G and subtract a smooth baseline to make the resonances more apparent; see Fig. 3(b). We then use a standard peak finding

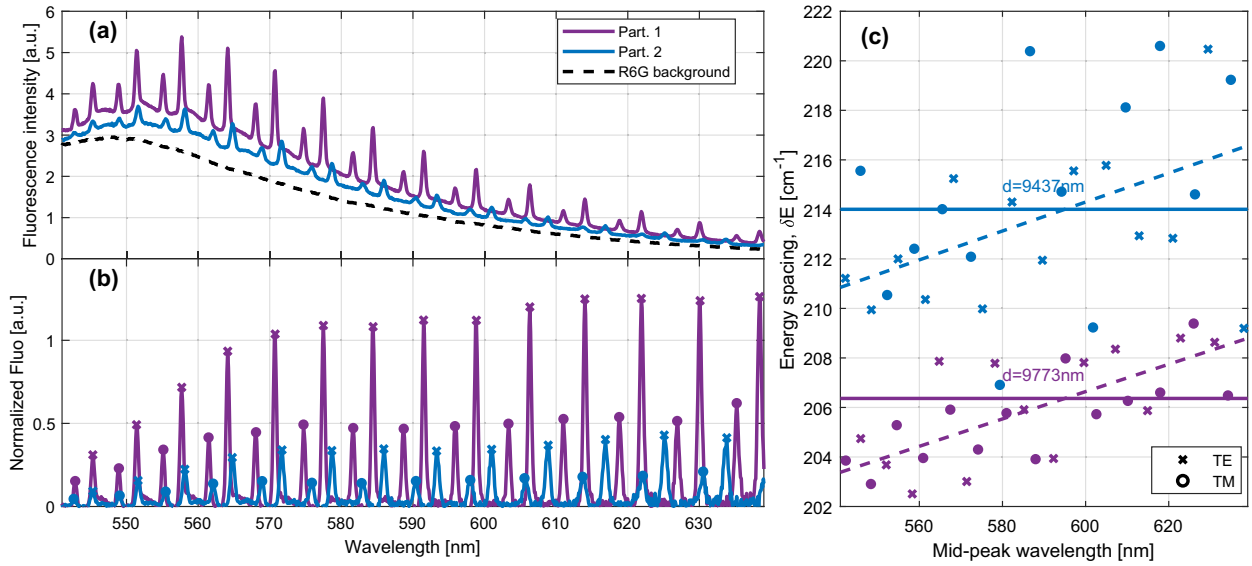

Fig. 3. (a) Example raw fluorescence spectra for two individual R6G-coated PS spheres of nominal 10 μm diameter excited at 514.5 nm, along with the fluorescence background of R6G in the absence of PS sphere (dashed line). (b) Normalized and background-corrected spectra and resonance positions as identified by the automatic peak-detection algorithm. Note that the peaks are alternating TE (crosses) and TM (circles) modes. (c) Mode spacing between consecutive TE and TM modes plotted against peak wavelength (averaged between the two peaks). The dashed lines are linear fits used to calculate the average δE (solid lines) from which the size is inferred using the relationship derived from Mie theory in Fig. 2(e).

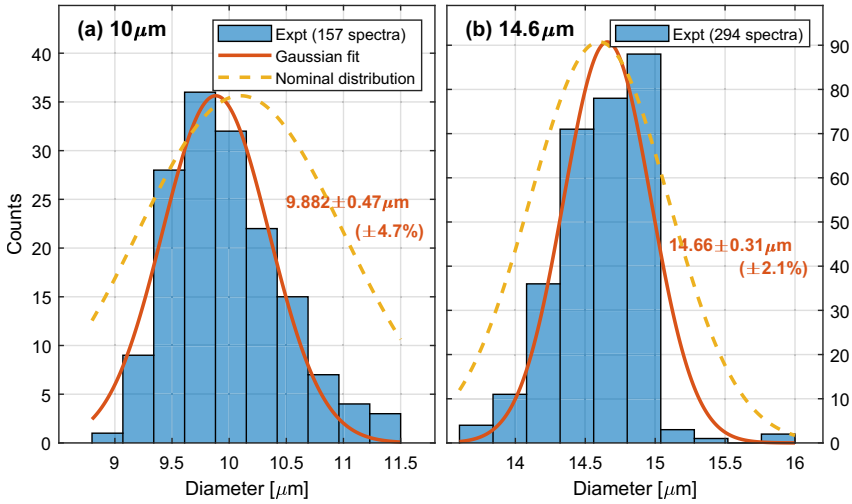

Fig. 4. Histogram of derived sizes for PS MSs in water of nominal diameter 10 μm (a) and 14.6 μm (b). The solid lines show a Gaussian fit to the data with the derived parameters given as $d_0 \pm \sigma$, where d_0 is the center diameter and σ the standard deviation. The nominal size distributions, 10.1 ± 0.9 μm (±8.9%) and 14.6 ± 0.5 μm (±3.4%) are plotted as dashed lines.

algorithm [such as `Findpeaks()` in MATLAB] to automatically extract peak positions. Parameters (peak linewidth, minimum peak spacing) are adjusted so that all WGM resonance peaks are detected, but it is then unavoidable that some additional peaks are sometimes registered in between, especially when the fluorescence is weaker. In order to remove these, we rely on the regular energy spacing between alternating peaks. Any peaks deviating from this behavior are then iteratively removed until all spacings are constant within a certain threshold.

D. Size Distribution

This algorithm, together with the simple size determination from the average energy spacing, allows us to easily analyze hundreds of dye-coated MS fluorescence spectra. In a typical set of 1000 acquisitions, we can identify around 10–15 separate single-MS events. Repeating this experiment 10 to 20 times, we can obtain sufficient statistics to study the size distribution of the MS solution. This is plotted as histograms in Fig. 4. We also fit Gaussian distributions to compare to the manufacturer specifications given as average diameter and standard deviation. The results are close to specifications, and we believe the discrepancy is likely due to the less accurate method used by the manufacturer to determine these parameters (typically dynamic light scattering). Our results also reveal the slightly non-Gaussian nature of these distributions.

4. DISCUSSION AND CONCLUSION

We now discuss a couple of possible sources of error in our measurement.

A. Dye-Concentration Dependence

The WGM resonances are very sensitive to their environment, notably to the refractive index of the surrounding medium. One could therefore expect that the adsorbed dye molecules slightly affect the resonance positions. One mitigating factor is that our method is based on mode spacing rather than absolute peak position. Nevertheless, in order to exclude any such issues, we have carried additional experiments at different dye concentrations. If the adsorbed dyes affect the mode spacing, then the derived sizes should be concentration dependent. The results for a 10 nM R6G concentration (10 times less than earlier) are shown in Fig. 5(a). This is a difficult experiment as we are comparing the size-distribution histogram for two different samples of the same population, so this will be affected by statistical fluctuations. Nevertheless, the results are sufficiently comparable to suggest that dye concentration does not affect the results (at least at the concentrations under consideration).

We can also attempt to justify this from a theoretical perspective. The adsorbed dye layer can be modeled as a continuous shell within an effective medium model [45]. Assuming a shell thickness of 1 nm and using the known polarizability of R6G [46], we can calculate the extinction spectrum of the PS core + dye shell system and deduce the expected shift in resonance, as shown in Fig. 5(b). This shows that WGM resonances around 600 nm are predicted to shift by only 0.25 nm or $\sim 7\ \mathrm{cm}^{-1}$ at a relatively high dye coverage of $\rho = 1\ \mathrm{nm}^{-2}$. Even then, mode spacing and inferred size are barely affected, with predicted changes of the order of 0.1% only. This justifies why our method is insensitive to any dye-induced shift of the resonances, especially given that we here used a maximum coverage of $0.25\ \mathrm{nm}^{-2}$ only.

B. Choice of Refractive Index

Another important parameter of the problem is the refractive index of PS. The refractive index of water is also important, but it has been measured with much greater accuracy, so we focus on PS. Many measurements of the refractive index of PS have been reported in the literature [40–42,47,48], as summarized in Table 1. Several of these reports closely agree with our choice [40], which strongly suggests that this is the best estimate. Data

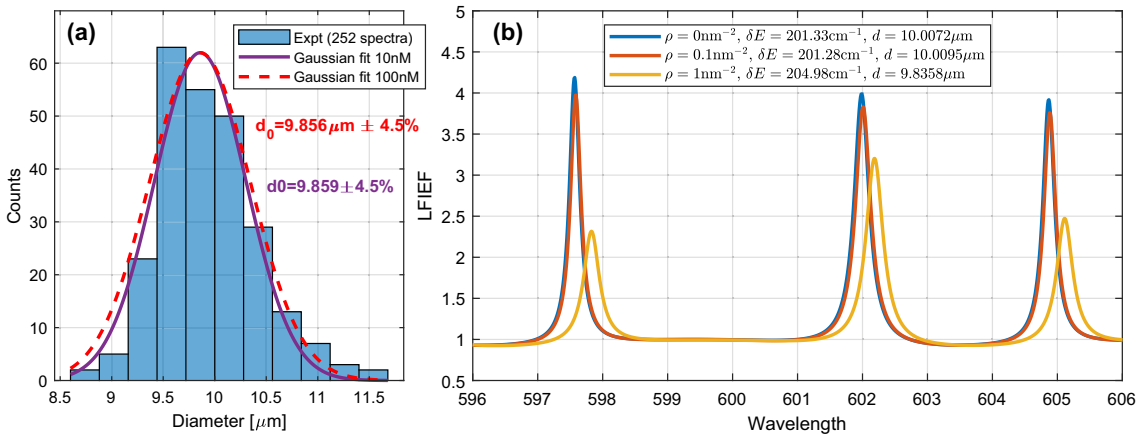

Fig. 5. (a) Histograms of sizes inferred from WGM resonances for 10 μm MS coated with a lower concentration 10 nM R6G. The distribution is the same within statistical uncertainty as for the higher concentration (100 nM), whose fit from Fig. 4 is shown as a dashed line. (b) Effective medium multilayer Mie theory [45] predictions of the WGM resonances for a 10 μm MS coated with increasing coverage ρ of R6G. The graph is zoomed on a small region for clarity, but the stated energy spacing between peaks (δE) is averaged over the range 550–640 nm as before. The diameters in the legend are as inferred from the quadratic relationship of Fig. 2(e). The effect of coverage on inferred size is largely negligible, even at a high coverage of 1 nm^{-2}.

inferred from polystyrene spheres in water [47] or in air [48] are slightly different to the other bulk measurement. It is likely that the discrepancy arises from the larger uncertainty in those methods, but it is also possible that the refractive index depends on the quality of the material and the fact that PS MSs might have a slightly different refractive index to bulk PS. We therefore try to assess this effect by repeating the Mie theory calculations with the different refractive index options and see how it affects the δE versus diameter relationship found in Fig. 2(e). This is summarized in Table 1. For similar refractive index data sets [40–42], the expected error is very small, 0.3%, and comparable to the uncertainty of the method anyway. The other two data sets [47,48] differ both in the absolute refractive index at 600 nm and the wavelength dependence characterized by the slope at 600 nm. In these cases, a systematic error by about 2% is expected. The manufacturer specifications for our particles are not accurate enough to be able to decide which data set is the most accurate in our case. In any case, an accuracy of 2%, together with a precision under 0.2%, will be sufficient in most applications. For example, size distributions are only affected by precision, not accuracy. Note however that these assumptions would need to be re-examined when applying the method to particles of different material or in different environmental conditions (such as another solvent).

C. Conclusion

In summary, we have presented in detail a method to determine the size of individual dielectric microspheres and deduce their size distribution. The method consists of coating the MSs with suitable dyes and measuring the fluorescence spectrum of many individual dye-coated MSs, which clearly reveal the WGM resonances. The mechanism enabling this observation is related to surface-enhanced fluorescence and a more detailed discussion of this aspect and the quantification of the fluorescence enhancements is outside the scope of this work but will be reported elsewhere. Focusing on the energy spacing between peaks, and using Mie theory, we can infer MS size with a high accuracy (∼0.2%). We have shown that the method agrees with manufacturer specifications within experimental uncertainty. This approach is not affected by dye concentration and only slightly depends on the choice of refractive index, so it is both robust and accurate. By its nature, the method relies on the observation of sharp WGM resonances, so its applicability is limited to systems exhibiting them, typically dielectric MSs in the range 5 to 20 μm in water, and down to ∼3 μm in air. We believe it could be used in a research context when determining the exact size of a particle is critical, or more routinely as quality control on solutions of dielectric microspheres. More broadly, it contributes to our fundamental understanding of WGM-supporting systems.

Funding. MacDiarmid Institute for Advanced Materials and Nanotechnology; Marsden Fund (VUW2118).

Table 1. Summary of Reported PS Refractive Indices and Their Effect on the WGM Size Determination Algorithm[a]

	n(600 nm)	$dn/d\lambda$(600 nm) [nm^{-1}]	Derived d [μm]	Error in d [%]
Eqn. 1 [40]	1.5881	0.0267	10.000	0
Ref. [41]	1.5902	0.0285	9.968	−0.3
Ref. [47]	1.5838	0.014	10.017	1.7
Ref. [48]	1.5572	0.0265	10.020	2.0

[a]The latter is calculated assuming $\delta E = 201.35\ cm^{-1}$, which corresponds to a diameter of exactly $d = 10$ μm for n given by Eq. (1).

Acknowledgment. ECLR thanks the Royal Society Te Apārangi for support through Marsden grants.

Disclosures. The authors declare no conflicts of interest.

Data availability. Data underlying the results presented in this paper are not publicly available at this time but may be obtained from the authors upon reasonable request.

Supplemental document. See Supplement 1 for supporting content.

REFERENCES

1. S. Freiberg and X. X. Zhu, "Polymer microspheres for controlled drug release," Int. J. Pharm. **282**, 1–18 (2004).
2. A. J. Durkin, S. Jaikumar, and R. Richards-Kortum, "Optically dilute, absorbing, and turbid phantoms for fluorescence spectroscopy of homogeneous and inhomogeneous samples," Appl. Spectrosc. **47**, 2114–2121 (1993).
3. R. T. Chartier and M. E. Greenslade, "Initial investigation of the wavelength dependence of optical properties measured with a new multi-pass aerosol extinction differential optical absorption spectrometer (AE-DOAS)," Atmos. Meas. Tech. **5**, 709–721 (2012).
4. F. Vollmer and S. Arnold, "Whispering-gallery-mode biosensing: label-free detection down to single molecules," Nat. Methods **5**, 591–596 (2008).
5. M. R. Foreman, J. D. Swaim, and F. Vollmer, "Whispering gallery mode sensors," Adv. Opt. Photonics **7**, 168–240 (2015).
6. G. C. Righini and S. Soria, "Biosensing by WGM microspherical resonators," Sensors **16**, 905 (2016).
7. T. Reynolds, N. Riesen, A. Meldrum, *et al.*, "Fluorescent and lasing whispering gallery mode microresonators for sensing applications," Laser Photonics Rev. **11**, 1600265 (2017).
8. H. Kawaguchi, "Functional polymer microspheres," Prog. Polym. Sci. **25**, 1171–1210 (2000).
9. A. Chiasera, Y. Dumeige, P. Féron, *et al.*, "Spherical whispering-gallery-mode microresonators," Laser Photonics Rev. **4**, 457–482 (2010).
10. D. S. Wiersma, "The physics and applications of random lasers," Nat. Phys. **4**, 359–367 (2008).
11. S. Kedia and S. Sinha, "Random lasing from dyed polystyrene spheres in disordered environments," J. Laser Appl. **30**, 032022 (2018).
12. M. B. Price, K. Lewellen, J. Hardy, *et al.*, "Whispering-gallery mode lasing in perovskite nanocrystals chemically bound to silicon dioxide microspheres," J. Phys. Chem. Lett. **11**, 7009–7014 (2020).
13. B. J. Berne and R. Pecora, *Dynamic Light Scattering (with Applications to Chemistry, Biology, and Physics)* (Dover, 2000).
14. H. Kato, A. Nakamura, K. Takahashi, *et al.*, "Accurate size and size-distribution determination of polystyrene latex nanoparticles in aqueous medium using dynamic light scattering and asymmetrical flow field flow fractionation with multi-angle light scattering," Nanomaterials **2**, 15–30 (2012).
15. G. Roll and G. Schweiger, "Geometrical optics model of Mie resonances," J. Opt. Soc. Am. A **17**, 1301–1311 (2000).
16. F. Azeem, M. R. Chaudhry, M. S. Anwar, *et al.*, "Optical whispering gallery mode resonators: analysing thermo-optic tuning in a silicon sphere," J. R. Soc. New Zealand, 1–25 (2024).
17. M. H. Humayun, I. Khan, F. Azeem, *et al.*, "Far-infrared elastic scattering proposal for the Avogadro project's silicon spheres," J. Quant. Spectrosc. Rad. Transf. **210**, 173–179 (2018).
18. T. Das, P. Ilaiyaraja, and C. Sudakar, "Whispering gallery mode enabled efficiency enhancement: defect and size controlled CdSe quantum dot sensitized whisperonic solar cells," Sci. Rep. **8**, 9709 (2018).
19. P. Chýek, "Partial-wave resonances and the ripple structure in the Mie normalized extinction cross section," J. Opt. Soc. Am. **66**, 285–287 (1976).
20. P. Chýlek, "Resonance structure of Mie scattering: distance between resonances," J. Opt. Soc. Am. A **7**, 1609–1613 (1990).
21. C. C. Lam, P. T. Leung, and K. Young, "Explicit asymptotic formulas for the positions, widths, and strengths of resonances in Mie scattering," J. Opt. Soc. Am. B **9**, 1585–1592 (1992).
22. P. Chýlek, J. Kiehl, and M. Ko, "Optical levitation and partial-wave resonances," Phys. Rev. A **18**, 2229 (1978).
23. P. Chýlek, V. Ramaswamy, A. Ashkin, *et al.*, "Simultaneous determination of refractive index and size of spherical dielectric particles from light scattering data," Appl. Opt. **22**, 2302–2307 (1983).
24. A. Ashkin and J. Dziedzic, "Observation of resonances in the radiation pressure on dielectric spheres," Phys. Rev. Lett. **38**, 1351 (1977).
25. A. Bain, A. Rafferty, and T. C. Preston, "Determining the size and refractive index of single aerosol particles using angular light scattering and Mie resonances," J. Quant. Spectrosc. Rad. Transf. **221**, 61–70 (2018).
26. S. H. Jones, M. D. King, and A. D. Ward, "Determining the unique refractive index properties of solid polystyrene aerosol using broadband Mie scattering from optically trapped beads," Phys. Chem. Chem. Phys. **15**, 20735–20741 (2013).
27. P. R. Conwell, C. K. Rushforth, R. E. Benner, *et al.*, "Efficient automated algorithm for the sizing of dielectric microspheres using the resonance spectrum," J. Opt. Soc. Am. A **1**, 1181–1187 (1984).
28. T. C. Preston and J. P. Reid, "Accurate and efficient determination of the radius, refractive index, and dispersion of weakly absorbing spherical particle using whispering gallery modes," J. Opt. Soc. Am. B **30**, 2113–2122 (2013).
29. T. C. Preston and J. P. Reid, "Determining the size and refractive index of microspheres using the mode assignments from Mie resonances," J. Opt. Soc. Am. A **32**, 2210–2217 (2015).
30. S. C. Hill, R. E. Benner, C. K. Rushforth, *et al.*, "Structural resonances observed in the fluorescence emission from small spheres on substrates," Appl. Opt. **23**, 1680–1683 (1984).
31. R. Benner, P. Barber, J. Owen, *et al.*, "Observation of structure resonances in the fluorescence spectra from microspheres," Phys. Rev. Lett. **44**, 475 (1980).
32. N. Riesen, T. Reynolds, A. François, *et al.*, "Q-factor limits for far-field detection of whispering gallery modes in active microspheres," Opt. Express **23**, 28896–28904 (2015).
33. S. Holler, N. L. Goddard, and S. Arnold, "Spontaneous emission spectra from microdroplets," J. Chem. Phys. **108**, 6545–6547 (1998).
34. P. G. Schiro and A. S. Kwok, "Cavity-enhanced emission from a dye-coated microsphere," Opt. Express **12**, 2857–2863 (2004).
35. E. C. Le Ru, E. Blackie, M. Meyer, *et al.*, "Surface enhanced Raman scattering enhancement factors: a comprehensive study," J. Phys. Chem. C **111**, 13794–13803 (2007).
36. C. F. Bohren and D. R. Huffman, *Absorption and Scattering of Light by Small Particles* (Wiley, 1983).
37. E. C. Le Ru and P. G. Etchegoin, "SERS and plasmonics codes (SPlaC)," Matlab codes freely available from http://www.vuw.ac.nz/raman/book/codes.aspx (accessed 1st August 2024).
38. E. C. Le Ru and P. G. Etchegoin, *Principles of Surface Enhanced Raman Spectroscopy and Related Plasmonic Effects* (Elsevier, 2009).
39. A. H. Harvey, J. S. Gallagher, and J. M. H. Levelt Sengers, "Revised formulation for the refractive index of water and steam as a function of wavelength, temperature and density," J. Phys. Chem. Ref. Data **27**, 761–774 (1998).
40. X. Zhang, J. Qiu, X. Li, *et al.*, "Complex refractive indices measurements of polymers in visible and near-infrared bands," Appl. Opt. **59**, 2337–2344 (2020).
41. I. D. Nikolov and C. D. Ivanov, "Optical plastic refractive measurements in the visible and the near-infrared regions," Appl. Opt. **39**, 2067–2070 (2000).
42. L. A. Matheson and J. L. Saunderson, *Optical and Electrical Properties of Polystyrene* (Reinhold, 1952).
43. E. C. Le Ru, P. G. Etchegoin, J. Grand, *et al.*, "Mechanisms of spectral profile modification in surface-enhanced fluorescence," J. Phys. Chem. C **111**, 16076–16079 (2007).
44. C. M. Galloway, P. G. Etchegoin, and E. C. Le Ru, "Ultrafast nonradiative decay rates on metallic surfaces by comparing surface-enhanced Raman and fluorescence signals of single molecules," Phys. Rev. Lett. **103**, 063003 (2009).

45. C. Tang, B. Auguié, and E. C. Le Ru, "Refined effective-medium model for the optical properties of nanoparticles coated with anisotropic molecules," Phys. Rev. B **103**, 085436 (2021).
46. A. Djorović, M. Meyer, B. L. Darby, *et al.*, "Accurate modeling of the polarizability of dyes for electromagnetic calculations," ACS Omega **2**, 1804–1811 (2017).
47. X. Ma, J. Q. Lu, R. S. Brock, *et al.*, "Determination of complex refractive index of polystyrene microspheres from 370 to 1610 nm," Phys. Med. Biol. **48**, 4165 (2003).
48. T. Galpin, R. T. Chartier, N. Levergood, *et al.*, "Refractive index retrievals for polystyrene latex spheres in the spectral range 220–420 nm," Aerosol Sci. Technol. **51**, 1158–1167 (2017).

130.195.253.53 (ja 2024-12-08 15:58:53)

Supplemental Document

applied optics

Dielectric microsphere sizing using fluorescence microscopy of whispering gallery mode resonances from adsorbed dyes: supplement

Azizeh Alidoust Ghatar, Nitay Ben-Shachar, and Eric C. Le Ru*

The MacDiarmid Institute for Advanced Materials and Nanotechnology, School of Chemical and Physical Sciences, Victoria University of Wellington, P.O. Box 600, Wellington 6140, New Zealand
eric.leru@vuw.ac.nz

This supplement published with Optica Publishing Group on 12 November 2024 by The Authors under the terms of the Creative Commons Attribution 4.0 License in the format provided by the authors and unedited. Further distribution of this work must maintain attribution to the author(s) and the published article's title, journal citation, and DOI.

Supplement DOI: https://doi.org/10.6084/m9.figshare.27613899

Parent Article DOI: https://doi.org/10.1364/AO.541870

Dielectric microsphere sizing using fluorescence microscopy of whispering gallery mode resonances from adsorbed dyes: supplemental document

S.I. EXTRACTING THE AVERAGE PEAK SPACING AND SIZE FROM EXPERIMENTAL OR THEORETICAL SPECTRA

We here provide more technical details on how the average peak spacing and particle size are found. We use the experimental spectrum of particle 1 in Fig. 3 for illustration. First, the peak positions are found using the algorithm described in the text for the region of interest (550 nm$\leq \lambda \leq$ 640 nm for 10 μm particles). Then we compute the spacings between alternating peaks (either TE or TM but the exact assignment does not matter). In our example, we have 15 TM peaks and 14 TE peaks, so we get 14 TM spacings, δ_M and 13 TE spacings, δ_E. For each pair of peaks, we also compute the center wavelengths. These spacings are plotted against center wavelengths in Fig. 3(c) for example. The distinction between TE and TM does not matter in the rest of the analysis, so we group these in 27 spacings δ_i and 27 center wavelengths λ_i. To find the average δE, we can simply take the average: $\delta E = \langle \delta_i \rangle$. In our example, this gives $\delta E = 206.26\,\mathrm{cm}^{-1}$. As an alternative, arguably more robust method, we can take a linear fit of the data δ_i vs λ_i, and calculate the fitted value at $\lambda = 595$ nm (mid point of our region of interest). The linear fit is shown as a dashed line in Fig. 3(c). This gives $\delta E = 206.36\,\mathrm{cm}^{-1}$, which is very close to the direct average result. For all our analyses, we have used the linear fit method but we believe the two are equivalent within experimental uncertainties.

Finally, in order to deduce the diameter d from the average δE, we use the quadratic relationship derived from Mie theory (using the same region of interest), as shown in Fig. 3(e):

$$\delta E = ad^2 + bd + c \tag{S1}$$

This can be solved for d:

$$d = \frac{-b + \sqrt{b^2 - 4a(c - \delta E)}}{2a} \tag{S2}$$

This gives $d = 9773$ nm in our example.

S.II. SUPPLEMENTARY FIGURES

Figs. S1 and S2 below are the equivalent of Figs. 2 and 3 in the main text, but focusing on 14.6 μm particles coated with Nile Blue instead of 10 μm with Rhodamine 6G.

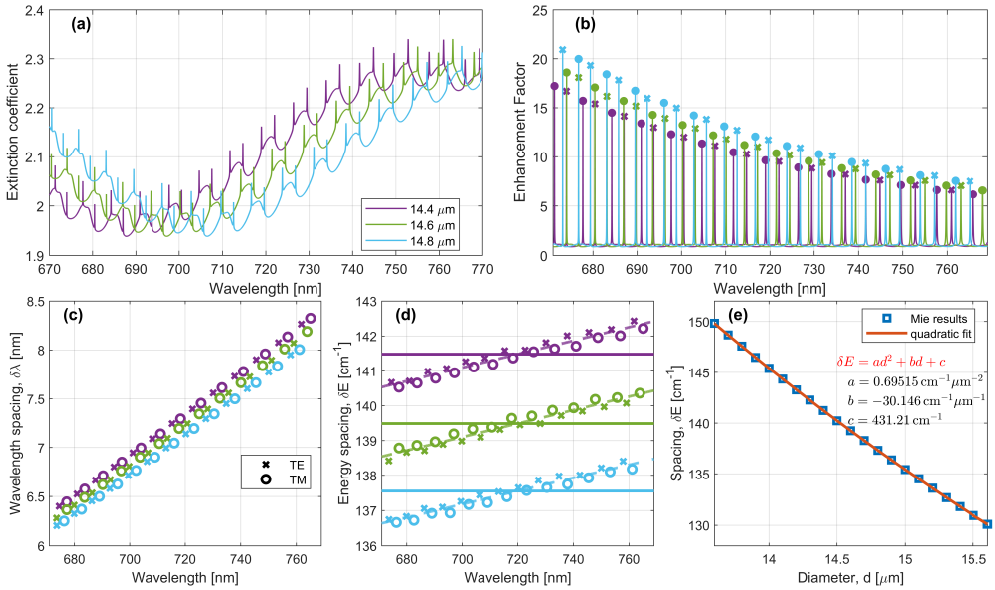

Fig. S1. (a-b) Calculated extinction spectra (a) and average local field intensity enhancement factor (b) for PS spheres of 14.4, 14.6, and 14.8 μm diameter in water. The derived location of the TE (x) and TM (o) resonances are indicated as symbols. (c-d) Wavelength (c) and energy (d) spacing between consecutive TE (x) or TM (o) resonances as a function of average peak wavelength for each particle. The energy spacing slightly increases linearly (dashed line show linear fit) and the average δE is shown as solid lines in (d). (e) Predicted δE as a function of particle size over the range $13.6 - 15.6\,\mu m$ and quadratic fit to the data.

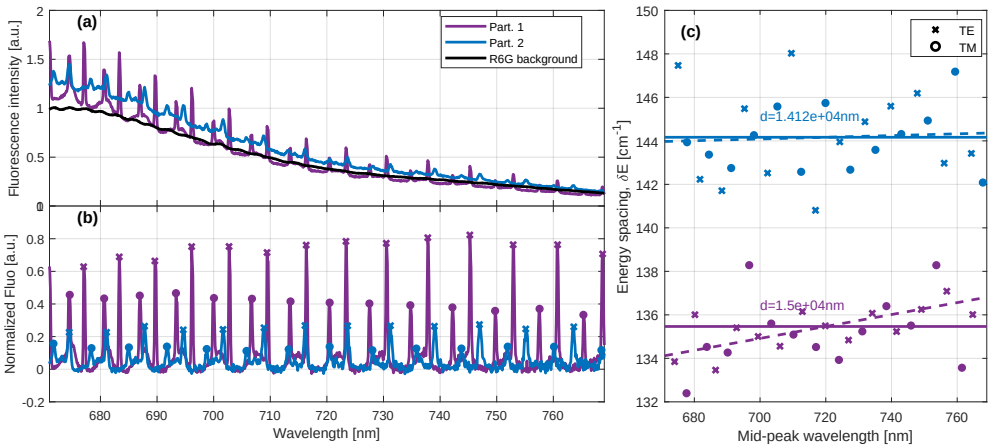

Fig. S2. (a) Example raw fluorescence spectra for two individual Nile-Blue-coated PS spheres of nominally 14.6 μm diameter excited at 632.8 nm, along with the fluorescence background of Nile Blue in the absence of PS sphere. (b) Normalized and background-corrected spectra and resonance positions as identified by the automatic peak-detection algorithm. Note that the peaks are alternating TE (crosses) and TM (circles) modes. (c) Peak spacing between consecutive TE (crosses) and TM (circles) modes plotted against peak wavelength (averaged between the 2 peaks). The dashed lines are linear fits used to calculate the average δE (solid lines) from which the size is inferred.